Phase Transitions of 4′-*n*-Hexacosyloxy-3′-nitrobiphenyl-4-carboxylic Acid (ANBC-26): Two Types of Thermotropic Cubic Phases

Shoichi Kutsumizu,*,† Tatsuya Ichikawa,‡ Minoru Yamada,‡ Shuichi Nojima,§ and Shinichi Yano‡

Instrumental Analysis Center, Gifu University, 1-1 Yanagido, Gifu 501-1193, Japan, Department of Chemistry, Faculty of Engineering, Gifu University, 1-1 Yanagido, Gifu 501-1193, Japan, and School of Materials Science, Japan Advanced Institute of Science and Technology (JAIST), 1-1 Asahidai, Tatsunokuchi, Nomi, Ishikawa 923-1292, Japan

Received: May 22, 2000; In Final Form: August 17, 2000

The phase transitions of 4′-*n*-hexacosyloxy-3′-nitrobiphenyl-4-carboxylic acid (ANBC-26, where "26" indicates the number of carbon atoms in the alkoxy group) were investigated by differential scanning calorimetric (DSC), polarizing optical microscopic, and X-ray diffraction (XRD) measurements. ANBC-26 is a new liquid crystalline material which exhibits successively two types of three-dimensionally ordered cubic mesophases on heating; the low-temperature cubic (CubI) phase has a space group of *Im*3*m*, and the high-temperature one (CubII phase) is of *Ia*3*d* type, identical with the cubic phase of shorter alkoxy chain homologues such as ANBC-16, and a cubic−cubic phase transition occurs at 435 K on DSC. Reversibility of the transitions between them was studied and the structures of those mesophases are discussed. The transformation from a one-dimensionally ordered smectic C (SmC) to the CubI phase and to the CubII phase can be interpreted qualitatively in terms of the increased curvature of the interface. The structured liquid I_1 phase, an intermediate phase between the CubII and a true isotropic liquid I_2 phases, has been also studied, indicating that this phase could be characterized by Ornstein−Zernike type short-range fluctuation, which means the presence of molecular clusters consisting of several ANBC-26 dimers in the temperature region.

1. Introduction

Cubic mesophases are in the limelight in the field of soft materials.[1−5] They are formed in a wide range of chemical systems, such as liquid crystals,[2] biological lipid−water,[3] and block copolymers.[4] The formation severely depends on temperature, the molecular structure, and composition; phase transitions between optically isotropic cubic phases and other optically anisotropic mesophases with lamellar or hexagonal columnar structure are still mysterious at several points. Regardless of the diversity of chemical systems, it is generally accepted that they consist of two incompatible components, e.g., aliphatic vs aromatic, apolar vs polar, or soft vs hard components, but our understanding in this field is far from complete.

4′-*n*-Alkoxy-3′-nitrobiphenyl-4-carboxylic acids (designated as ANBC-*n*, where *n* is the number of carbon atoms in the alkoxy group, see Chart 1in the Experimental Section) have been investigated by several researchers[6−30] and are well-known for forming a cubic phase labeled cubic D (CubD) in a certain temperature range. The alkoxy chain length *n* is a key factor for determining the phase behavior; when $n \geq 16$, the CubD phase appears on both heating and cooling and its temperature region becomes wider with increasing *n* (to $n = 26$);[6,7,11,19,29] $n = 15$ is a critical length of the alkoxy chain, where the formation of the CubD phase is severely affected by thermal cycles used.[26,29] The phase transition from a lamellar smectic C (SmC) to the CubD phase (and vice versa) brings about dramatic changes in physical properties in addition to the optical property, and the storage modulus jumps about 1000 times at the transition to show a value of the order of 10^7 dyn/cm^2 in the CubD phase region.[20,26] ANBC-*n* has a relatively simple molecular structure which consists of a biphenylcarboxylic acid core, a nitro group at the side, and a long alkoxy tail, where the carboxylic acid group is known to be hydrogen-bonded with other molecules to dimerize.[21,29] Such simple molecular structure would be advantageous when the molecular organization within the cubic lattice and the factors by which the phase formation is governed are considered.

The molecular organizations in such mesophases are usually investigated by X-ray diffraction measurements.[9,10,14,16,18,23,28,30] For the $n = 16$ and 18 homologues, the structure type of the CubD phase has been already identified as space group *Ia*3*d*.[10,18,23] By aid of other physical measurements such as NMR[15,22] or dynamic viscoelastic measurements,[20,26] it is now accepted that the structure of the CubD phase is a bicontinuous type, where the rod micelles are connected 3-by-3 to form two sets of interwoven networks, according to Luzzati and Spect's rod-connectors scheme[33] (see the upper part of Figure 6). A somewhat surprising fact[23] is that a 3′-cyano analogue with $n = 18$ (4′-*n*-octadecyloxy-3′-cyanobiphenyl-4-carboxylic acid, ACBC-18) shows a different type of structure with space group *Im*3*m*, and the cubic structure is severely dependent on its molecular structure.

Very recently, we have found that one ANBC homologue having a very long alkoxy chain of $n = 26$ successively forms two types of cubic phases, one with *Im*3*m* symmetry and the other with *Ia*3*d*, and the *Im*3*m* cubic phase is transformed into

* Author to whom correspondence should be addressed. E-mail: kutsu@cc.gifu-u.ac.jp.
† Instrumental Analysis Center, Gifu University.
‡ Department of Chemistry, Faculty of Engineering, Gifu University.
§ School of Materials Science, Japan Advanced Institute of Science and Technology (JAIST).

10.1021/jp0018652 CCC: $19.00
Published on Web 10/13/2000

the *Ia*3*d* cubic phase at 435 K on heating.[28] This is the first example of thermotropic cubic−cubic phase transition in one-component systems, although two examples have been reported in lyotropic binary or ternary mixtures, where the phase behavior is a function of water content.[3,31,32] For a fundamental understanding of this transition, detailed investigation of the phase structures is prerequisite, and in this work, the lamellar SmC-to-*Im*3*m* cubic and the *Im*3*m* cubic-to-*Ia*3*d* cubic phase transitions are greatly paid attention to. The results of thermogravimetric and differential scanning calorimetric studies, optical microscopic observation, and X-ray diffraction studies by using a high-resolution small-angle X-ray scattering (SAXS) instrument are presented, and the molecular organizations of the *Im*3*m*-cubic (denoted as CubI in this paper), *Ia*3*d*-cubic (CubII), and a structured liquid labeled I_1, which is an intermediate phase between the CubII and a true isotropic liquid (I_2), are discussed.

2. Experimental Section

Preparation. *Preparation of Hexacosyl Bromide (BA-26).*[34,35] First, a Grignard reagent ($C_{16}H_{33}MgBr$) was prepared in the following manner. Magnesium turnings (0.04 mol) were covered with a mixture of 1,2-dibromoethane (0.1 mL) and anhydrous ethyl ether (30 mL) under a dry N_2 gas atmosphere and stirring was begun, to which a mixed solution of hexadecyl bromide (0.04 mol) and anhydrous ethyl ether (20 mL) was added dropwise. Next, the Grignard reagent prepared was added dropwise to a stirred anhydrous tetrahydrofuran (THF) solution (50 mL) of lithium tetrachlorocuprate(II) (0.0004 mol) and 1,10-dibromodecane (0.04 mol) in an iced bath, where lithium tetrachlorocuprate(II) was prepared by mixing $CuCl_2$ (0.0004 mol) with LiCl (0.0008 mol) in anhydrous THF (20 mL). The reaction solution was stirred for an additional 24 h, and after that, water was added to remove the metal residue into the water layer. Finally, the organic layer was filtered to give a white solid of hexacosyl bromide ($C_{26}H_{53}Br$, BA-26), which was recrystallized from ethanol several times until the melting temperature reached a constant value of 56 °C.[36] The purity was checked by thin-layer chromatography (TLC), ^{1}H nuclear magnetic resonance (^{1}H NMR), mass spectroscopy (MS), and differential scanning calorimetry (DSC).

Preparation of ABC-26 and ANBC-26. 4′-*n*-Hexacosyloxybiphenyl-4-carboxylic acid (ABC-26) was prepared by reacting BA-26 obtained above with 4′-hydroxybiphenyl-4-carboxylic acid, and then nitration of ABC-26 gave ANBC-26. These two processes were based on the established method of Gray et al.[6,37] The final white powder product was purified by repeated recrystallization from ethanol, and the purity was checked by elemental analysis, TLC, ^{1}H NMR, MS, and DSC. Yield, about 50%.

δ_H (400 MHz, solvent $CDCl_3$, standard TMS): 0.88 (a, t, ^3J = 6.8 Hz, 3H), 1.25 (b, m, 44H), 1.50 (c, qn, ^3J = 6.9 Hz, 2H), 1.87 (d, qn, ^3J = 7.6 Hz, 2H), 4.16 (e, t, ^3J = 6.5 Hz, 2H), 7.18 (f, d, $^3J_{fg}$ = 9.0 Hz, 1H), 7.67 (i, d, $^3J_{ij}$ = 8.5 Hz, 2H), 7.79 (g, d,d, $^3J_{gf}$ = 8.8 Hz, $^4J_{gh}$ = 2.4 Hz, 1H), 8.12 (h, d, $^4J_{hg}$ = 2.4 Hz, 1H), 8.18 (j, d, $^3J_{ji}$ = 8.5 Hz, 2H); *m*/*z* 624 (M^+, 3.7%), 494 (2.8%), 259 (88.3%), 43 (100%). MS spectra did not detect the mass fragment larger than 624 even when an extremely concentrated solution was used, indicating no content of longer alkoxy or alkyl chain byproducts than C_{26}. The elemental analysis for ANBC-26 was carried out by the laboratory for Organic Elemental Microanalysis of Kyoto University, giving a result well consistent with its formula: Anal. Calcd for $C_{26}H_{53}NO_5$: C, 75.12; H, 9.97; N, 2.25; O, 12.84. Found: C, 74.93; H, 9.99; N, 2.20; O, 12.86%.

CHART 1

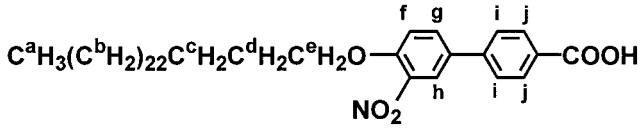

Measurements. The IR spectra were recorded on a Perkin-Elmer 1640 and a Perkin-Elmer system 2000 Fourier transform IR spectrometer. The ^{1}H NMR and MS spectra were recorded on a JEOL JNM-α400 spectrometer and a Shimadzu GCMS QP-1000 system, respectively. The phase transitions and thermal stability were examined on a Seiko Denshi DSC-210 and TG/DTA-300 interfaced to a TA data station (SSC 5000 system). The measurements at a scanning rate of 5 K min^{-1} were performed under a dry N_2 flow of ca. 40 mL min^{-1} for DSC and of ca. 200 mL min^{-1} for TG/DTA. The texture of each mesophase was observed at a heating/cooling rate of 5 K min^{-1} by using a Nikon Optiphot-pol XTP-11 polarizing optical microscope (POM) equipped with a Mettler FP-82 hot stage and a Mettler FP80 central processor.

X-ray diffraction (XRD) patterns at elevated temperatures were obtained for powder samples filled in thin glass capillaries with 1.5 mm diameter (Hilgenberg Co.), which were placed in a Mettler FP82HT hot stage, and the temperature was controlled within ±0.1 °C by a Mettler FP90 central processor. The accuracy of the temperature was checked by using a calibrated Fe-constantan thermocouple. The following two setups were used.

(A) A MAC Science X-ray generator (M18XHF) was operated with a copper target at 40 kV and 30 mA, and the Cu Kα radiation (λ = 0.154 nm) was point-focused with Huxley-Holms optics. The scattered X-ray was detected by a one-dimensional position-sensitive proportional counter (PSPC) with an effective length of 10 cm. The distance between the sample and PSPC was about 40 cm, and the geometry was further checked by a chicken tendon collagen, which gives a set of sharp diffractions corresponding to 65.3 nm, and α-stearic acid giving a set of diffractions of 3.962 nm. The accumulation time for each measurement was 500−3600 s, depending on the intensity and the quality needed.

(B) A Rigaku R-AXIS IIC X-ray system was used and operated with a copper target at 40 kV and 150 mA, and the Cu Kα radiation was collimated into the sample capillary. The scattered X-ray was recorded on a two-dimensional imaging plate (IP) detector with an effective area of 20 × 20 cm^2, and the sample-to-detector distance was 20 cm. The exposure time for each measurement was 5−10 min.

Results

ANBC-26 synthesized was first studied by thermogravimetry (TG) and was found to be thermally stable; no weight loss was detected up to 500 K, which was the highest temperature used in the present studies. Even at 550 K, about 80 K higher than the clearing temperature, only a 0.3% loss was observed, much less than that for ANBC-16 (1.4% loss at 550 K). Hence, lengthening of the alkoxy chain from n = 16 to 26 resulted in a fair improvement of thermal stability of ANBC-*n* homologues, which is of course very important for the detailed investigations of ANBC-26.

Figure 1 shows the DSC trace of ANBC-26 at a heating/cooling rate of 5 K min^{-1}. Phase transition temperatures and enthalpy changes are listed in Table 1. On first heating (1H), ANBC-26 melts at 376 K into a smectic C (SmC) phase,

TABLE 1: Transition Temperatures (in K) and Transition Enthalpies (in kJ mol^{-1}) of ANBC-26[a]

run	Cr_1/Cr'		Cr_2/Cr		SmC		CubI		CubII		Hex		I_1		I_2
1H	•	359 [38.8]	•	376 [46.7]	•	396 [2.2]	•	435 [0.1]	•			467 [4.1]	•	473 [6.9]	•
1C	•			349 [−47.1]	•	366 [−4.6]			•	462 [−1.9]	•	465 [−1.4]	•	471 [−6.9]	•
2H	•	352 [−2.2]	•	376 [46.0]	•	395 [2.2]	•	436 [0.1]	•			467 [3.6]	•	472 [8.8]	•

[a] 1H, first heating; 1C, first cooling; 2H, second heating. Phases marked • appear on each run.

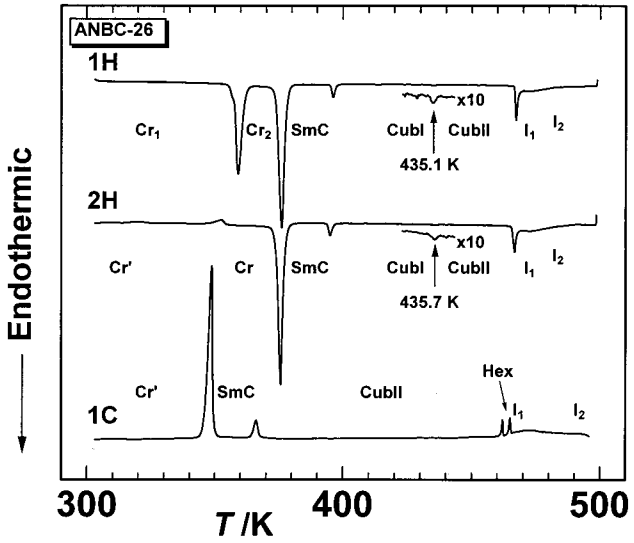

Figure 1. DSC traces measured at 5 K min^{-1} for ANBC-26. 1H, 2H, and 1C mean the first and second heating, and first cooling runs, respectively. Cr, crystalline; SmC, smectic C; Cub, cubic; Hex, hexagonal columnar; I, isotropic liquid phases.

characterized by the appearance of a typical SmC schlieren texture under crossed polarizers, and then undergoes a SmC-to-cubic phase transition at 396 K, readily identified by slow growth of completely black and thus optically isotropic domains with straight edges. Initially, one type of cubic phases was thought to range up to 467 K, but looking closer at the heating trace, a faint endothermic peak is visible at 435 K, around at a mid temperature of the cubic phase region. The enthalpy change estimated ($\sim$0.2 J g^{-1} = 0.1 kJ mol^{-1}) is barely beyond the noise level of our DSC instrument used, and the peak was also observed at 436 K on the second heating (2H). The XRD results later described indicate that this is due to a cubic-to-cubic phase transition, and hereafter, the low- and high-temperature cubic phases are denoted as CubI and CubII, respectively, as shown in the figure. At 467 K, a sharp endothermic peak is seen, followed by a broad hump centered at 473 K. The XRD measurements showed the destruction of the CubII lattice at 467 K, but there still remains a broad but distinct peak in the small-angle region, suggesting the presence of some organization between the two temperatures. The state of this temperature region is thus assigned to a structured liquid, labeled I_1 in the figure. The structure of the I_1 phase will be discussed later, in the Discussion section (see Figure 9). At around 473 K, the small-angle XRD peak virtually disappeared, indicating that the sample changes into a genuine isotropic liquid (I_2). On 2H scan, the sample showed crystallization of residual glassy regions at 352 K, but was otherwise identical with 1H scan.

On cooling (1C) from 498 K, there was observed a broad exothermic peak centered at 471 K, and after that two sharp exothermic peaks appear at 465 and 462 K. Between the two temperatures, as shown in Figure 2, a pseudo-focal conic texture was observed on POM, indicative of a hexagonal columnar

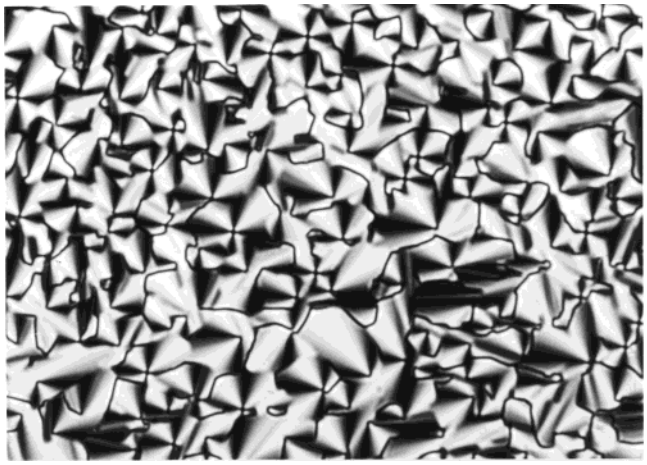

Figure 2. Photomicrograph of the Hex phase of ANBC-26 at 458.8 K, at which the CubII phase should appear on DSC because the temperature region of the Hex phase is 462−465 K in the DSC cooling; there exists a small discrepancy with temperature.

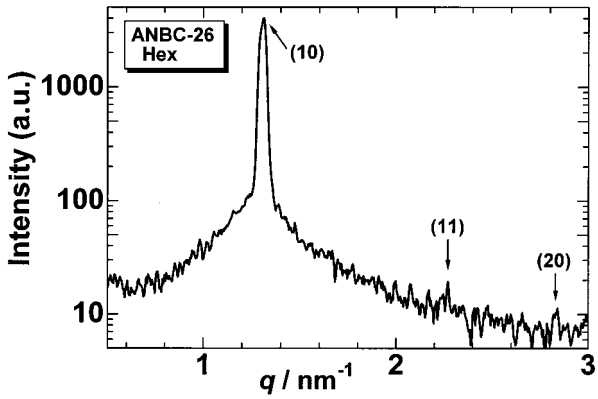

Figure 3. SAXS pattern of the Hex phase of ANBC-26 recorded at 465 K on cooling. The indexation (*hk*) are also shown.

(Hex) mesophase.[38] The XRD pattern recorded at 465 K is shown in Figure 3, where a strong diffraction peak at 1.31 nm^{-1} and two very weak peaks at 2.27 and 2.83 nm^{-1} are seen. Here, $q = (4\pi/\lambda)\sin\theta$, $\lambda = 0.154$ nm, and 2θ = scattering angle. The ratios of the reciprocal spacings are $\sqrt{1}:\sqrt{3}:\sqrt{4}$, corresponding to the indexation (hk) = (10), (11), and (20) of the Hex phase with a lattice parameter of $a = 5.52$ nm. Below 462 K (457.9 K on POM observation; see the caption for Figure 2), the texture suddenly turned to completely black, showing the formation of a cubic phase, and on further cooling, no definite peaks were observed until the sample shows a SmC phase at 366 K. Consequently, the phase sequence of the cooling process is hexagonal columnar-cubic-lamellar SmC in going from higher temperature, reminiscent of the phase sequence often seen in lyotropic liquid crystalline systems exhibiting a cubic phase, although in the latter systems it is a function of the amount of solvent.

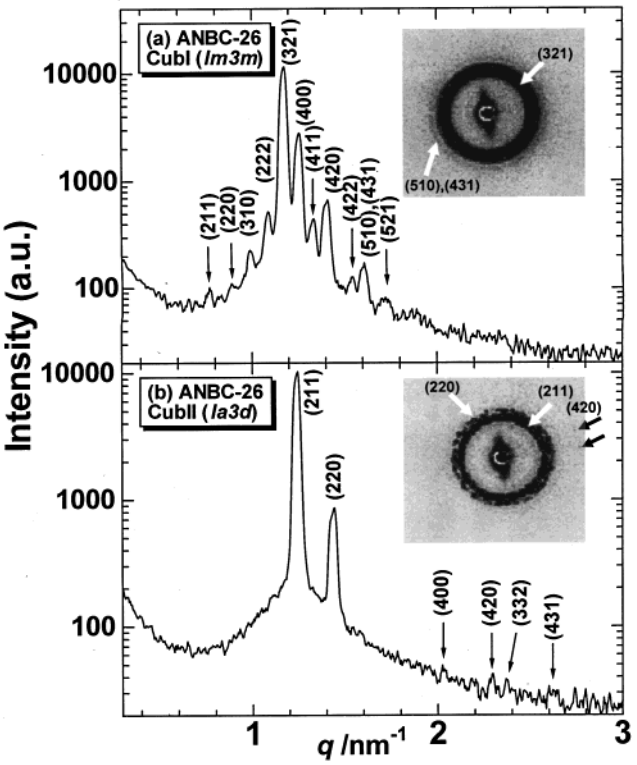

Figure 4. SAXS patterns of two cubic phases of ANBC-26 recorded at (a) 404 K and (b) 444 K, on heating. Corresponding two-dimensional patterns are shown in the inset. Miller indices are also shown in the figure.

Figure 4 shows XRD patterns in the small-angle region of ANBC-26 detected by PSPC at two different temperatures below and above the temperature at which the DSC faint peak was observed on heating. The corresponding IP patterns are also presented in the insets. Although it is not so obvious in the IP patterns, the two PSPC patterns are clearly different. At 404 K in Figure 4a, 11 peaks are observed with the following ratios of reciprocal spacings: $\sqrt{3}$:$\sqrt{4}$:$\sqrt{5}$:$\sqrt{6}$:$\sqrt{7}$:$\sqrt{8}$:$\sqrt{9}$:$\sqrt{10}$:$\sqrt{12}$:$\sqrt{13}$:$\sqrt{15}$. Since the ratios $\sqrt{7}$ and $\sqrt{15}$ are not compatible with any cubic lattices, the sequence of numbers must be doubled. Thus, the obtained ratios are $\sqrt{6}$:$\sqrt{8}$:$\sqrt{10}$:$\sqrt{12}$:$\sqrt{14}$:$\sqrt{16}$:$\sqrt{18}$:$\sqrt{20}$:$\sqrt{24}$:$\sqrt{26}$:$\sqrt{30}$, which is characteristic of a body-centered cubic symmetry, most probably *Im*3*m*, and thus the parameter of the unit cell of the CubI phase is $a = 20.02 \pm 0.02$ nm. Table 2 summarizes the indexing. The pattern of the CubI phase was arranged almost symmetrically with respect to the beam stopper (not shown here), which well corresponds to the observation of diffraction **rings** on the IP image in the inset. On heating, the PSPC pattern abruptly changed at around 428 K, slightly lower than the corresponding temperature on DSC, and at 444 K, in Figure 4b, two strong peaks with the ratio $\sqrt{6}$:$\sqrt{8}$ and very weak peaks corresponding to the ratio $\sqrt{16}$:$\sqrt{20}$:$\sqrt{22}$:$\sqrt{26}$ are seen. Although not shown in this figure, the pattern was very often dissymmetric with respect to the beam stopper. Correspondingly, the IP pattern recorded at the same temperature consists of many **spots**, arranged into two rings denoted as (211) and (220). These observations clearly reflect an improved growth of CubII domains compared to the case of the CubI phase in the glass capillary tube. Since ANBC-26 is achiral, only a space group *Ia*3*d* matches the absence of diffractions with lower indices (100), (110), (111), (200), and (210). The cell parameter is $a = 12.30 \pm 0.04$ nm (see Table 2). The high-temperature CubII phase has the same symmetry as the CubD phase of ANBC-16[10] and -18[18,23] previously reported. In fact, the PSPC pattern obtained for the CubII phase of ANBC-26 is quite similar to that reported for the CubD phase of ANBC-18.[23] On the other hand, the low-temperature CubI phase and the cubic phase of a 3′-cyano analogue, ACBC-18,[23] are of the same type. Finally, it should be noted that the use of a high-resolution SAXS equipment in the present work was essential to the finding of two types of cubic phases in the cubic phase temperature region of ANBC-26.

What is the type of the cubic phase on cooling? To clarify this, we used the IP patterns because in the cubic temperature region on cooling the PSPC patterns detected only a strong reflection peak, as shown in Figure 3, from which it is difficult to identify the type definitely. Figure 5 presents the IP patterns

TABLE 2: X-ray Diffraction Data of Two Cubic Phases of ANBC-26[a]

	CubI at 404 K space group *Im*3*m*, $a = 20.02 \pm 0.02$ nm		CubII at 444 K space group *Ia*3*d*, $a = 12.30 \pm 0.04$ nm	
hkl	d_{calc}	d_{obs}	d_{calc}	d_{obs}
110	14.155		abs	
200	10.009		abs	
211	8.172	8.199	5.020	5.004
220	7.077	7.100	4.347	4.361
310	6.330	6.350	abs	
222	5.779	5.745	abs	
321	5.350	5.334	3.286	
400	5.004	4.997	3.074	3.09
411	4.718	4.701	abs	
420	4.476	4.484	2.749	2.75
332	4.268		2.621	2.65
422	4.086	4.080	2.510	
510/431	3.926	3.928	2.411*	2.39
521	3.655	3.667	2.245	

[a] a (in nm) is the cubic cell parameter. d_{calc} and d_{obs} (in nm) are the calculated and observed spacings of the (*hkl*) small-angle reflections, respectively; abs, systematic absences of reflections determined by each space group; *, only the (431) reflection is observable.

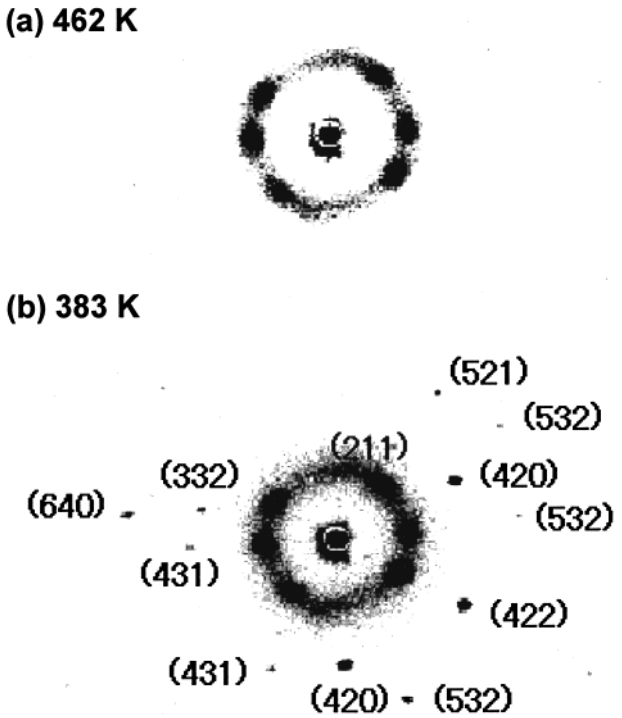

Figure 5. Two-dimensional SAXS patterns of ANBC-26 recorded at (a) 462 K and (b) 383 K on cooling. In (b), Miller indices are also shown.

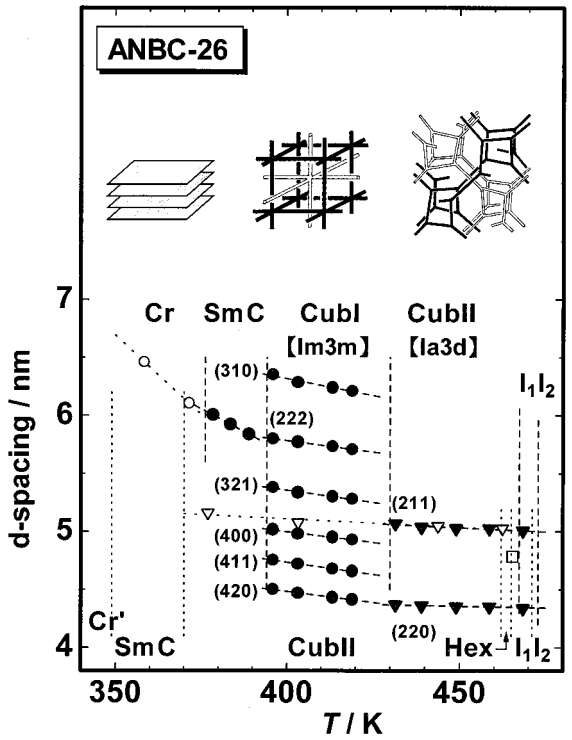

Figure 6. Plots of *d* spacing versus temperature for ANBC-26; filled and open symbols represent the data recorded on heating and cooling, respectively. The model structures of SmC, CubI, and CubII phases are shown in the upper part of this figure.

on cooling. The patterns on cooling are spot-like, rather than in rings, reflecting a strong tendency for the formation of larger domains compared to the case on heating. As the temperature decreased, the spots sharpened and the number detected increased, but the pattern itself was unchanged. At 383 K, in Figure 5b, the pattern containing the largest number of spots was obtained, and the indexing is consistent with the *Ia*3*d* symmetry of the CubII phase. Thus, we concluded that the cubic phase on cooling is the CubII phase alone.

To get insight into the transformation process along the SmC−CubI (*Im*3*m*)−CubII (*Ia*3*d*) phase sequence on heating, the *d* spacings of the diffraction peaks (filled symbols) are plotted versus temperature in Figure 6, which also contains the data on cooling (open symbols). The schematic models for the three structures are depicted in the upper part of this figure. The structures of two cubic phases are based on the models proposed for lyotropic systems by Luzzati and co-workers,[3,33] where white and black skeletons only depict the central lines of the rods (or correspond to the core parts of the rod micelles), not the rod micelles themselves. In ANBC-26, the aromatic part and COOH group are considered to be at around the white and black skeletons, and the aliphatic chain fills out the free space between them.

Several interesting points are noted: (1) The layer thickness of the SmC phase decreases as the temperature approaches the SmC-to-CubI phase transition temperature. When the SmC layer is transformed into the SmA layer, the tilt angle of the molecular long axis against the layer normal usually goes to zero and thus the layer thickness increases, as in the case of ANBC-14[39] (which shows no cubic phase). Therefore, the "thinning" of the SmC layers may be characteristic of the SmC phase that exhibits any cubic phase at the higher temperature side. The largest magnitude of the decrease in layer thickness (L_{SmC}) was obtained ($dL_{SmC}/dT = 1.6 \times 10^{-2}$ nm K^{-1}) for ANBC-26, while for ANBC-15 with a minimum length of the alkoxy chain for showing a cubic phase, $dL_{SmC}/dT = 7 \times 10^{-4}$ nm K^{-1}, the smallest among the ANBC-*n* homologues examined.[39]

(2) Rançon and Charvolin[40] studied the phase transitions of hexaethylene glycol mono-*n*-dodecyl ether ($C_{12}EO_6$)/water system and pointed out the existence of epitaxial relationships between particular planes of three successive phases: the layer of the lamellar phase, the (211) plane of the *Ia*3*d* cubic phase, and the (10) plane of the hexagonal columnar phase. These three planes are of highest density of matters in each of the three phases, and the relations themselves demonstrate the direct transformations of a highest density plane into other at the phase transitions, when the temperature or the amount of water is varied.

For ANBC-26, the SmC layer thickness is almost equal to the (222) spacing of the CubI phase with *Im*3*m* symmetry at the SmC-to-CubI phase transition on heating, suggesting the existence of such an epitaxial relation. This is of course only a suggestion because we did not use an oriented sample, but this relation seems to have the following physical meaning. In the *Im*3*m* cubic phase with a cell parameter *a*, one 6-by-6 connection point is located at (000), the other being at (*a*/2,*a*/2,*a*/2), and the distance between them is ($\sqrt{3}$)*a*/2, while the (222) spacing is described as ($\sqrt{3}$)*a*/6. Here, the line connecting between (000) and (*a*/2,*a*/2,*a*/2) is normal to the (222) planes. Hence, three layers should exist between the two connection points. The structure of the CubI phase will be discussed later in detail. On the other hand, the (321) spacing versus temperature curve of the CubI phase and the (211) spacing versus temperature curve of the CubII phase show a discontinuity at the CubI-to-CubII phase transition, where both planes are the highest intensity plane of each.

(3) On cooling (open symbols in Figure 6), the sequence of mesophases in ANBC-26 is the same in $C_{12}EO_6$/water system, irrespective of the reverse order in the latter in the temperature scale. However, in ANBC-26, a small but distinct discontinuity is seen at the Hex-to-CubII phase transition, and at the CubII-to-SmC phase transition temperature, then, a large discrepancy was observed between the SmC layer thickness and CubII (211) spacing. On the other hand, the temperature curve of the (211) spacing on cooling gave a straight line down to the CubII-to-SmC phase transition, superimposed with the curve on heating. This also confirms the appearance of only one type in the cubic region on cooling.

Figure 7 shows plots of the cubic cell parameters as a function of temperature. What is noteworthy is that in the CubI phase temperature range, the unit cell parameter *a* decreases with increasing temperature, showing a *negative* thermal volume expansion ($(1/a^3)(\partial(a^3)/\partial T) = -2.3 \times 10^{-3}$ K^{-1}). This trend continues but is greatly reduced (-6.6×10^{-4} K^{-1}) when temperature goes into the CubII phase temperature range. The CubII phase on cooling also showed a negative thermal expansion (-8.4×10^{-4} K^{-1}). Bruce et al. reported such a negative thermal volume expansion (-1.5×10^{-3} K^{-1}) for the *Ia*3*d* cubic phase of a silver(I)−alkoxystilbazole complex.[41] Paleos et al. also reported that in dialkyl phosphate potassium salts the thermal expansion of the *Ia*3*d* cubic phase is negative, -1.2×10^{-3} K^{-1} for the octyl to -3.0×10^{-3} K^{-1} for the octadecyl derivative.[42] It seems that the negative thermal volume expansion is characteristic of cubic mesophases. Provided that the density is unchanged with temperature (and assumed to be 1), the negative thermal volume expansion in the case of ANBC-26 implies that the number of molecules per unit cell decreases

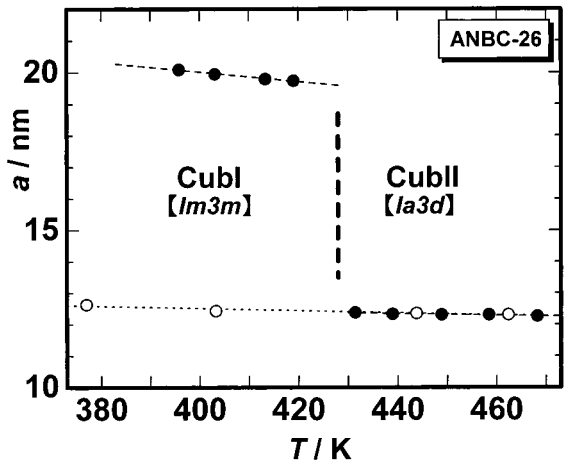

Figure 7. Temperature dependence of the unit cell parameters *a* of the CubI and CubII phases; filled and open symbols represent the data on heating and cooling, respectively. Vertical dashed line is the cubic−cubic phase transition temperature determined by SAXS experiments.

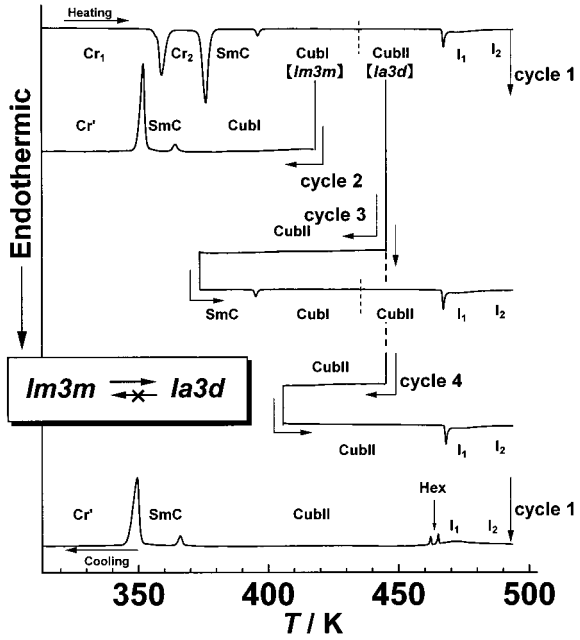

Figure 8. DSC traces (5 K min^{-1}) of ANBC-26, recorded under various thermal cycles. Cycle 1, heated to 498 K in the I_2 phase, and cooled to 293 K; cycle 2, heated to 413 K in the CubI phase, and cooled to 293 K; cycle 3, heated to 448 K in the CubII phase, cooled to 373 K at which the CubII phase was observed, and heated again to 498 K; cycle 4, heated to 448 K in the CubII phase, cooled to 403 K, a temperature at which the CubI phase would be observed on heating, and heated again to 498 K. Notations of phases are the same as in Figure 1.

with increasing temperature; for example, the number estimated decreases by 6% from 396 to 419 K in the CubI phase region, which can be said to reflect a *fluid* nature of the cubic phase. In hexagonal columnar mesophases, a similar negative thermal expansion was reported in the direction perpendicular to the column,[43,44] but not known whether the expansion is also negative along the columnar direction.

A question arises whether the CubI phase is metastable. To answer this question, we investigated the phase behavior of ANBC-26 under different thermal cycles, by using DSC, POM, and XRD. The result is shown in Figure 8. The cycle 1, heating to and cooling from 498 K in the I_2 phase region, is our routine DSC measurement for ANBC-*n* homologues, the result of which has already been described in Figure 1. When heating was stopped at 413 K in the CubI phase region and the cooling was started, cycle 2, the CubI phase was maintained during the cooling to 364 K, at which the SmC phase appeared. The CubI-to-SmC phase transition temperature on this cooling is almost the same with the CubII-to-SmC phase transition temperature (366 K) on cooling in cycle 1; the transition enthalpy was 3.2 kJ/mol, 30% smaller than the CubII-to-SmC transition enthalpy (4.6 kJ/mol). Moreover, annealing at a temperature in the CubI phase for 1 h or 1 day did not change the XRD pattern. These results conclude that the CubI phase is not a metastable phase.

In cycle 3, the cycle was reversed at 448 K in the CubII phase, and the CubII phase was observed on the cooling to 373 K. At 373 K, reheating was begun, and then, the transformation to the SmC phase quickly took place. After that, the phase behavior was identical with that in cycle 1, instead of the fact that the CubI-to-CubII phase transition was located at a temperature between 423.4 and 439.9 K by XRD but not detected by DSC. In cycle 4, the heating was stopped at 448 K to start the cooling, as in cycle 3, but unlike cycle 3, reheating was begun at 403 K, at which the CubI phase would be observed on heating. However, the CubII phase was maintained on the reheating as well as the preceding cooling, and even after annealing at 408 K (still in the CubI phase region on heating) for 1 h. These results suggest an interesting fact that the CubI phase can be formed from the SmC phase on heating, but the transformation from CubII to CubI phase does not occur.

Discussion

Structure of the CubII Phase with *Ia*3*d* Symmetry. For the *Ia*3*d* cubic structure illustrated in the upper part of Figure 6, the diameter (D) and the length (L) of the constituent rods and the number of molecules (N) per unit length of the rod are approximately evaluated by the following equations:[30,33]

$$D = (\sqrt{5}/4)a \quad (1)$$

$$L = a/(\sqrt{8}) \quad (2)$$

$$N = \rho a^3 N_A/24M \quad (3)$$

where a is the unit cell parameter, N_A Avogadro's number, M molecular mass, and ρ the density (which is assumed to be 1 g/cm^3 ($=10^{-21}$ g/nm^3)). The values of D, L, and N were estimated for three ANBC-*n* homologues, ANBC-16, -18, and -26, and are 5.82 nm, 3.68 nm, and 15.8 nm^{-1} for $n = 16$ (at 457 K), and 6.04 nm, 3.82 nm, and 16.7 nm^{-1} for $n = 18$ (at 455 K), and 6.88 nm, 4.35 nm, and 17.2 nm^{-1} for $n = 26$ (at 449 K), respectively. D and L increase linearly with the alkoxy chain length n, whereas N is almost constant with n.[30] In the wide-angle region of the XRD pattern,[30] three cubic phases showed a diffuse halo originating in a short-range correlation of about 0.4 to 0.5 nm, corresponding to the average transverse distance between ANBC-*n* molecules. It is thus visualized that each slice of the rod with a thickness of ~0.4 nm contains about three ANBC-*n* dimers for $n = 16$, 18, and 26. This molecular picture within the rod micelles of the cubic phase was first proposed by Guillon and Skoulios for $n = 16$,[45] and the present work has revealed that their model is realized independent of n for all ANBC-*n* homologues. Consequently, the structure of the CubII phase and its molecular organization of ANBC-26 are essentially the same as those of $n = 16$ and 18, except for the size aspect of the rod micelles, which is governed by the alkoxy chain length n.

Structure of the I_1 Phase. Figure 9 shows XRD patterns (open circles) as a function of temperature in the vicinity of

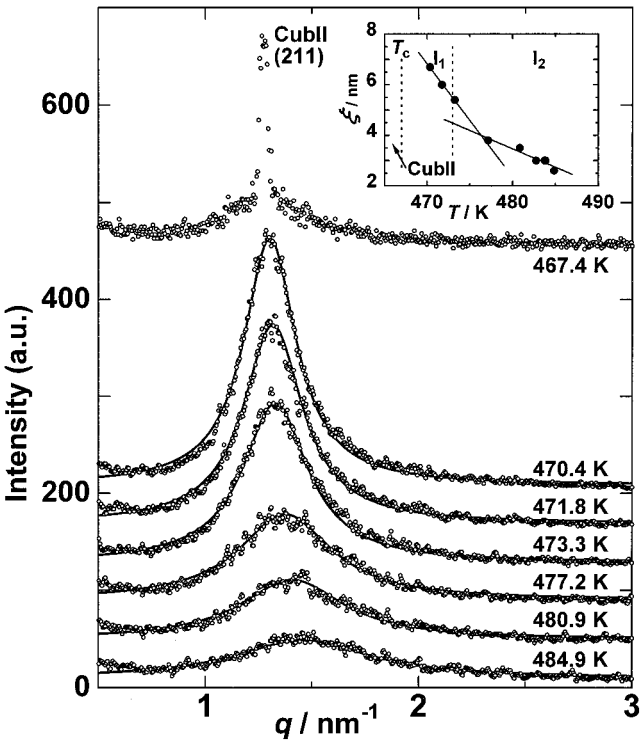

Figure 9. SAXS patterns (open circles) as a function of temperature in the vicinity of the CubII-to-I_1 phase transition temperature and above on heating. The solid curves represent the fit by the Ornstein-Zernike type function (see text), and the inset shows the temperature dependence of the correlation length ξ (filled circles) as obtained from the fits.

the CubII-to-I_1 phase transition temperature and above. At the CubII-to-I_1 phase transition (at 467 K by DSC, T_c), a sharp (211) reflection peak observed in the CubII temperature region disappeared to leave a broad halo at around $q = 1.4$ nm^{-1}. As temperature increases, this halo becomes broader, initially rapidly in the temperature region of the I_1 phase and into the I_2 temperature region gradually. As shown as solid curves in the figure, this halo was reproduced well by the following Ornstein-Zernike type function,[46,47]

$$I(q) = I(q^*)/[1+\xi^2(q - q^*)^2] \quad (4)$$

where ξ is the correlation length associated with a short-range fluctuation and q^* is the q value at which the halo shows a maximum. Here, the halo is so broad that instrumental smearing is negligible. The inset plots the values of ξ obtained from the fits as a function of temperature. The plots are roughly divided into two straight lines, which are crossed at 476 K, slightly higher temperature than the I_1-to-I_2 phase transition temperature determined by DSC (473 K). At temperatures in the I_1 phase, the value of ξ is of the order of 6 nm, close to the diameter D of rod micelles constructing the CubII lattice (described above), which strongly suggests the existence of molecular clusters probably containing several ANBC-*n* dimers in each. Into the I_2 phase region, then, the value of ξ is around 3−4 nm, almost corresponding to the distance between two neighboring ANBC dimers, which is in good agreement with the fact that this phase is a normal isotropic liquid.

In connection with a broad hump observed by DSC above the clearing temperature T_c, the assignment of the I_1 phase of ANBC-*n* homologues with shorter alkoxy chains such as $n =$ 16 has long been attracted and disputed.[11,13,19,21,22,24,25,48] For example, Goodby et al.[48] tried to explain this phase in terms of "lattice melting"; they considered that the CubD phase is made up of spherical micelles and leaves the remnants of the CubD lattice or clusters of ANBC-*n* molecules in the next I_1 phase before the complete melting. The possibility of the existence of such weak organization in the I_1 phase was supported by the XRD studies, which were first carried out by Gray et al. for $n = 16$[13] and recently by us for $n = 15$, 18−20, 22, and 26 also.[30] The XRD photos exhibit a sharp diffraction ring at a small angle, corresponding to a spacing ∼30% shorter than the length of ANBC-*n* dimer, together with a diffuse ring at a wide angle. In the present work, the former small-angle ring was observed as a halo at $q = q^*$ in Figure 9, and the temperature dependence of the correlation length has provided more clear evidence of a weak organization in the I_1 phase and its vanishing into the I_2 phase.

In A−B diblock copolymer systems, a similar phenomenon termed *correlation hole effect* has often been seen in a short temperature interval above the order−disorder transition temperature, where it is explained that each chain forms a globule with a radius of gyration R_g, not so much entangled with other chains, and thus the density fluctuations with the distance scale larger than R_g are virtually reduced by the conformational constraint, bringing about a scattering peak at q^* ($\sim 1/R_g$).[49−51] In the present low-molecular-mass system, the same type of globules would be formed only by the aggregation of several ANBC-*n* dimers, that is, the formation of molecular clusters. Strictly speaking, the I_1 phase is not a liquid but should be assigned reasonably to an intermediate phase leading to a true liquid phase, just like Blue phases[52] in cholesteric liquid crystalline materials, and so the code "I" may not be appropriate. However, it is worth noting that the reverse process from the I_2 to the I_1 phase on cooling exhibits an exothermic DSC peak corresponding to the endothermic peak on heating (see Figure 1), and the I_1 phase should not be discarded as a pretransitional effect.

Structure of the CubI Phase with *Im*3*m* Symmetry. On the basis of rod-connectors models illustrated in Figure 6, a difference between *Im*3*m* and *Ia*3*d* cubic structures lies in the way the constituent rods are connected to form a network, and at first sight, the phase transition from the CubI phase with symmetry *Im*3*m* to the CubII phase with symmetry *Ia*3*d* might be regarded as a simple re-combination of those rods from 6-by-6 to 3-by-3 connections. With the same concept, the number of connecting rods for the SmC phase may be regarded as ∞, and 0 for the I_1 phase, and thus, this concept seems to be reasonable in that the number decreases successively along with the phase sequence of SmC−CubI−CubII−I_1 on heating. The reality is, however, not so simple, and the size aspect of the rods in the CubI phase is not the same as that in the CubII phase.

As already mentioned, in the CubI phase with a lattice constant of a, the distance between two 6-by-6 connection points, for example, between (000) and (a/2,a/2,a/2), is very close to **three** times SmC layer thickness. Here, one SmC layer thickness corresponds to one dimer length of ANBC-26 whose alkoxy chains would be thermally shrunk (or curled). It is, therefore, suggested that in the CubI phase, each rod with a diameter roughly corresponding to the ANBC-26 dimer length is enrobed with an additional layer of ANBC-26 dimers, if we wish to preserve the rod-connectors model. A similar molecular organization picture has been proposed by Levelut and Clerc for an *Im*3*m* cubic phase of ACBC-18.[23] They postulated that the location of methyl end groups constitutes three continuous surfaces; one was described by the so-called infinite periodic

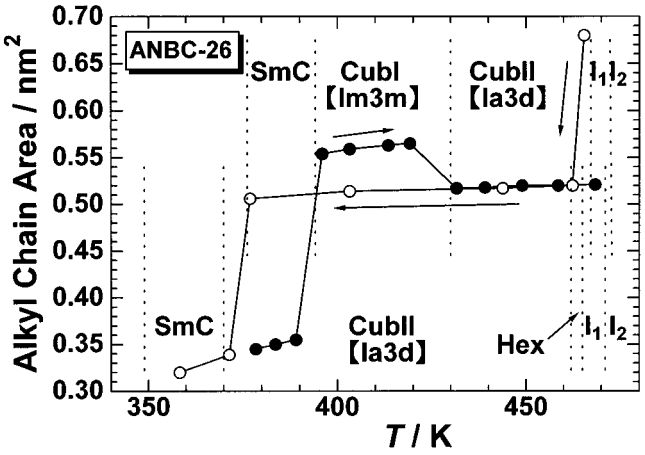

Figure 10. Temperature dependence of alkyl chain area in nm^2; filled and open symbols represent the data recorded on heating and cooling, respectively. Sections shown in the upper and lower parts represent the phase transition temperatures on heating and cooling, respectively.

minimal surface (IPMS)[53−56] of type P (P-surface), and the other two were constructed by a space foliation,[57] where the latter two correspond to *inner* surfaces of the **doubled circular rods** and sandwich the former P-surface. The total interface area (S), which is the sum of the areas of three surfaces, was computed to result in the relation $S = 5.39a^2$, whereas the corresponding relation for an *Ia*3*d* cubic IPMS (G-surface) is $S = 2.453\ 2^{1/3}a^2 = 3.091a^2$.[53,56] Provided that all the surfaces are continuous everywhere in the unit cell as usually postulated for IPMS, the minimum layer thickness encountered within their cubic cell model is $a/6$ (= 3.3 nm), which seems too narrow compared with the ANBC-26 dimer length (8.5 nm) and the SmC layer thickness (~6 nm), even if the "curling" of the alkoxy chains is taken into consideration. At this point, their model is somewhat questionable, and also in our model, it is more probable that the diameter of the rod is not constant but modulated in the longitudinal direction. Probably, the real cubic phase has some defects at which the surface is discontinuous. Anyway, if we notice that the CubI phase still has some regions of lamellar-like (but not lamellar) structure in the outside layer of the doubled circular rods, it is reasonable that the *Im*3*m*-CubI phase is an intermediate structure between the SmC lamellar and the *Ia*3*d*-CubII structures. Qualitatively, this implies that the average curvature of the methyl end surfaces of the *Im*3*m*-CubI phase lies between those of the SmC (which is 0) and the *Ia*3*d*-CubII phases (see also Figure 11).

Phase Transitions from the SmC to the CubI and from the CubI to the CubII Phase. With analogy of the formation of lyotropic cubic phases, one driving force to deform the SmC lamellar structure might be considered thermal motion of alkyl chain ends, which increases the actual bulkiness with increasing temperature.[5] The alkyl chain area (A) is a parameter reflecting such thermal motion, defined by Levelut and Fang[18] as

$$A = S/(N_0/2) \tag{5}$$

where S is the total surface area covered by methyl end groups and N_0 is the number of the methyl groups present at both sides of the surface; such surface is called *mean* surface (between two interfacial surfaces) by Charvolin,[58] or *neutral* surface by Caffrey et al.[59] Figure 10 shows plots of the estimated alkyl chain area as a function of temperature, where the relation $S = 5.39a^2$ was used for the estimation in the CubI phase region, although this model is actually one option for the *Im*3*m*-CubI phase.

The temperature variation of the alkyl chain area (A) on cooling is monotonic and the obtained trend A(SmC) < A(CubII) < A(Hex) in going from lower temperature is reasonable. Here, the area in the SmC phase is denoted as A(SmC) and the areas for other phases likewise. On heating, however, A(CubI) is slightly (~10%) larger than A(CubII) of the CubII phase that appears at the high-temperature side, but considering the situation on selecting the model for the *Im*3*m*-CubI phase, the result may be regarded as an indication of A(CubI) ≈ A(CubII). Hence, the formation of the CubI phase between the SmC and CubII phases could be understood in terms of mean surface area governed by thermal motion.

How do we understand the fact that the *Im*3*m*-CubI structure can be formed from the preceding SmC layer structure on heating but not from the *Ia*3*d*-CubII structure on cooling? In thermotropic liquid crystalline systems, there have been several reports revealing that the formation of cubic phases is strongly affected by the preceding phase structure on thermal cycle. Strontium stearate has an alkyl chain extending at both sides of the −COOSrOOC− core part, very similar to the alkoxy chains of ANBC-26 dimer. This compound is well-known for exhibiting an *Ia*3*d* cubic phase (usually labeled Q) in a certain temperature range on both heating and cooling,[33] but it was recently revealed that the phase formed on cooling from a hexagonal columnar phase (labeled H) is more dynamically *disordered* than that formed from a rhombohedral phase (labeled R) on heating.[60] In the ANBC-*n* homologue with $n = 15$, where the length of the alkoxy chain is critical for forming the CubD phase with *Ia*3*d* symmetry, the appearance itself is strongly affected by thermal cycles used.[26] A hydrazine derivative, 1,2-bis(4-*n*-octyloxybenzoyl)hydrazine, exhibits a cubic phase with *Ia*3*d* on both heating and cooling and it was pointed out that the formation of nuclei of the cubic structure in the preceding phase would be important for the appearance of the phase.[61] These dependences of cubic formation on the thermal cycle, not seen for lyotropic liquid crystalline systems, may be characteristic of thermotropic liquid crystalline systems, especially **one-chain** systems with a long aliphatic chain at each terminal.

To understand such characteristic of one-chain systems and confirm our hypothesis, the structural investigation of a binary system of ANBC-14 and *n*-hexadecane is of much interest. As expected from a report by Sorai, Saito, and their collaborators for a binary system of ANBC-16 and *n*-tetradecane,[24] in the ANBC-14-*n*-hexadecane system, *n*-hexadecane as well as the alkoxy chain of ANBC-14 act as a solvent to fill the remaining space outside the core parts of rod micelles in the cubic structure and contribute to the effective number n^* of carbon atoms when the system is regarded as a one-component system. In fact, it has been found that the phase diagram with respect to n^* is very similar to that of pure ANBC-*n* system versus n. In the binary system, the aliphatic component played by both *n*-hexadecane and the alkoxy chain of ANBC-14 would occupy the space more freely, without any conformational restriction; the re-organization on varying temperature would be regarded simply as a process of change in the interface such as a layer deformation, not requiring to take the interactions within "layer" into consideration. The investigation using XRD is in due course in our laboratories and will be published elsewhere.

Concluding Remarks

Despite the very simple chemical structure of ANBC-26, the polymorphism is very unique and includes two cubic mesophases with *Im*3*m* and *Ia*3*d* symmetries on heating and a weak organization made up of the *Ia*3*d* lattice remnants in the I_1 phase.

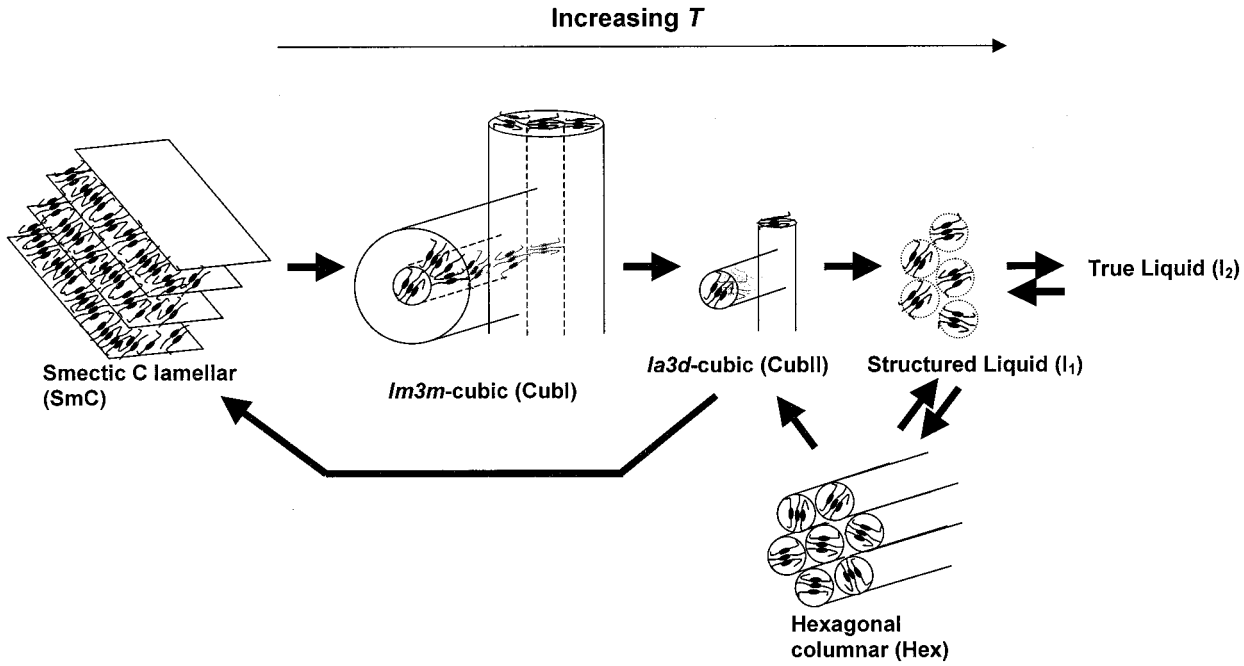

Figure 11. Schematic phase behavior of ANBC-26.

The reverse transition from the *Ia*3*d*-CubII to the *Im*3*m*-CubI phase could not be observed on cooling, and instead, a Hex phase newly appears above the temperature region of the *Ia*3*d*-CubII phase. Figure 11 summarizes the change of molecular organization of ANBC-26 on varying temperature (*T*).

The structure of the *Ia*3*d*-CubII phase is depicted as two sets of interwoven networks of rod micelles each of which is connected 3-by-3. The diameter of the rod micelles roughly corresponds to the length of ANBC-26 dimer, and the molecular organization is well understood by the picture proposed by Guillon and Skoulios.

The structure of the *Im*3*m*-CubI phase remains to be further reflected on, but at this stage, it is considered that this cubic phase has also a paired network structure of rod micelles, where the rods are connected 6-by-6 and each rod is a doubled circular rod, that is, a rod with a diameter roughly corresponding to the dimer length of ANBC-26 is enrobed with an additional layer of ANBC-26 dimers. The outer layer may be regarded as more lamellar-like than the inner rod, and in this respect, the *Im*3*m*-CubI phase is an intermediate structure between the SmC lamellar and *Ia*3*d*-CubII phases. In other words, qualitatively, the average curvature of the methyl end surfaces of the *Im*3*m*-CubI phase lies between those of the SmC and the *Ia*3*d*-CubII phases.

It is worth noting that high-resolution SAXS experiments are essential for distinguishing different types of cubic phases, and thus, the cubic region of ANBC-*n* homologues other than ANBC-26 may include more than one type of cubic phases, which is currently being reinvestigated in our laboratories.

We have also shown in this paper that the I_1 phase could be characterized by Ornstein-Zernike type short-range fluctuation, indicating the presence of molecular clusters consisting of several ANBC-26 dimers in this phase. At this point, this phase is an intermediate state into a true isotropic liquid I_2.

In ANBC-*n* homologues, the simple molecular shape would be advantageous when more detailed theoretical considerations are made, and thus we anticipate that our findings in the present work will lead to more complete understanding of cubic molecular organization and its transformation to and from other types, especially in thermotropic liquid crystalline systems.

Acknowledgment. We thank Dr. Satoshi Tanimoto at JAIST for his kind help with the X-ray experiment using IP, and Prof. Keiichi Moriya at Gifu University for his valuable experimental suggestions. Thanks are also due to Ms. Yumiko Murase and Eri Kumita at Instrumental Analysis Center, Gifu University, for the measurements of MS spectra. This work was partly supported by the Research Foundation for the Electrotechnology of Chubu (R-11123). We are also grateful to the two reviewers for their careful reading of the manuscript and for their constructive criticism.

References and Notes

(1) de Gennes, P.-G. *Angew. Chem., Int. ed. Engl.* **1992**, *31*, 842.
(2) Diele, S.; Göring, P. In *Handbook of Liquid Crystals*; Demus, D., Goodby, J., Gray, G. W., Spiess, H.-W., Vill, V., Eds; Wiley-VCH: Weinheim, 1998; Vol. 2B, pp 887−900.
(3) Mariani, P.; Luzzati, V.; Delacroix, H. *J. Mol. Biol*. **1988**, *204*, 165.
(4) Bates, F. S.; Fredrickson, G. H. *Annu. Rev. Phys. Chem.* **1990**, *41*, 525.
(5) Israelachvili, J. N. *Intermolecular and Surface Forces*; Academic Press: London, 1985.
(6) Gray, G. W.; Jones, B.; Marson, F. *J. Chem. Soc.* **1957**, 393.
(7) Demus, D.; Kunicke, G.; Neelsen, J.; Sackmann, H. *Z. Naturforsch.* **1968**, *23a*, 84.
(8) Pelzl, G.; Sackmann, H. *Symp. Chem. Soc., Faraday Division* **1971**, *5*, 68.
(9) Diele, S.; Brand, P.; Sackmann, H. *Mol. Cryst. Liq. Cryst.* **1972**, *17*, 163.
(10) Tardieu, A.; Billard, J. *J. Phys. (Paris) Coll.* **1976**, *37*, C3−79.
(11) Demus, D.; Marzotko, D.; Sharma, N. K.; Wiegeleben, A. *Krist. Tech.* **1980**, *15*, 331.
(12) Gray, G. W.; Goodby, J. W. *Smectic Liquid Crystals*; Leonard Hill: Glasgow, 1984; pp 68−81, including also earlier references on thermotropic cubic phases.
(13) Gray, G. W. In Zehn Arbeiten uber Flüssige Kristalle; Kongress- und Tagung-berichte der Martin-Luther-Universität; Halle-Wittenberg, 1986; pp 22−42.
(14) Etherington, G.; Leadbetter, A. J.; Wang, X. J.; Gray, G. W.; Tajbakhsh, A. *Liq. Cryst.* **1986**, *1*, 209.
(15) Ukleja, P.; Siatkowski, R. E.; Neubert, M. E. *Phys. Rev.* **1988**, *A38*, 4815.
(16) Etherington, G.; Langley, A. J.; Leadbetter, A. J.; Wang, X. J. *Liq. Cryst.* **1988**, *3*, 155.
(17) Billard, J.; Zimmermann, H.; Poupko, R.; Luz, Z. *J. Phys. (Paris)* **1989**, *50*, 539, including references on other types of thermotropic cubic phases.

(18) Levelut, A.-M.; Fang, Y. *Coll. Phys., Coll.* **1990**, *51*, C7−229.
(19) Kutsumizu, S.; Yamada, M.; Yano, S. *Liq. Cryst.* **1994**, *16*, 1109.
(20) Yamaguchi, T.; Yamada, M.; Kutsumizu, S.; Yano, S. *Chem. Phys. Lett.* **1995**, *240*, 105.
(21) Kutsumizu, S.; Kato, R.; Yamada, M.; Yano, S. *J. Phys. Chem., B* **1997**, *101*, 10666.
(22) Tansho, M.; Onoda, Y.; Kato, R.; Kutsumizu, S.; Yano, S. *Liq. Cryst.* **1998**, *24*, 525.
(23) Levelut, A.-M.; Clerc, M. *Liq. Cryst.* **1998**, *24*, 105.
(24) Saito, K.; Sato, A.; Sorai, M. *Liq. Cryst.* **1998**, *25*, 525.
(25) Sato, A.; Saito, K.; Sorai, M. *Liq. Cryst.* **1999**, *26*, 341.
(26) Kutsumizu, S.; Yamaguchi, T.; Kato, R.; Yano, S. *Liq. Cryst.* **1999**, *26*, 567.
(27) Sato, A.; Yamamura, Y.; Saito, K.; Sorai, M. *Liq. Cryst.* **1999**, *26*, 1185.
(28) Kutsumizu, S.; Ichikawa, T.; Nojima, S.; Yano, S. *Chem. Commun.* **1999**, 1181.
(29) Kutsumizu, S.; Yamaguchi, T.; Kato, R.; Ichikawa, T.; Yano, S. *Mol. Cryst. Liq. Cryst.* **1999**, *330*, 359.
(30) Kutsumizu, S.; Kobayashi, H.; Nakamura, N.; Ichikawa, T.; Yano, S.; Nojima, S. *Mol. Cryst. Liq. Cryst.*, in press.
(31) Longley, W.; McIntosh, T. J. *Nature* **1983**, *303*, 612.
(32) Larsson, K. *Nature* **1983**, *304*, 664.
(33) Luzzati, V.; Spegt, P. A. *Nature* **1967**, *215*, 701.
(34) Tamura, M.; Kochi, J. *Synthesis* **1971**, 303.
(35) Friedman, L.; Shani, A. *J. Am. Chem. Soc.* **1974**, *96*, 7101.
(36) Nakamura, N.; Watanabe, A. *Yukagaku* **1976**, *25*, 485 (in Japanese).
(37) Gray, G. W.; Hartley, J. B.; Jones, B. *J. Chem. Soc.* **1955**, 1412.
(38) Destrade, C.; Foucher, P.; Gasparoux, H.; Nguyen, H. T.; Levelut, A.-M.; Malthete, J. *Mol. Cryst. Liq. Cryst.* **1984**, *106*, 121.
(39) Kutsumizu, S.; Ichikawa, T.; Nojima, S.; Yano, S. Unpublished results.
(40) Rançon, Y.; Charvolin, J. *J. Phys. Chem.* **1988**, *92*, 2646.
(41) Donnio, B.; Heinrich, B.; Gulik-Krzywicki, T.; Delacroix, H.; Guillon, D.; Bruce, D. W. *Chem. Mater.* **1997**, *91*, 2951.
(42) Paleos, C. M.; Kardassi, D.; Tsiourvas, D.; Skoulios, A. *Liq. Cryst.* **1998**, *25*, 267.
(43) Zamir, S.; Singer, D.; Spielberg, N.; Wachtel, E. J.; Zimmermann, H.; Poupko, R.; Luz, Z. *Liq. Cryst.* **1996**, *21*, 39.
(44) Artzner, F.; Veber, M.; Clerc, M.; Levelut, A.-M. *Liq. Cryst.* **1997**, *23*, 27.
(45) Guillon, D.; Skoulios, A. *Europhys. Lett.* **1987**, *3*, 79.
(46) Feigin, L. A.; Svergun, D. I. *Structure Analysis by Small-Angle X-ray and Neutron Scattering*; Plenum Press: New York, 1987; p 243.
(47) de la Cruz, M. O.; Sanchez, I. C. *Macromolecules* **1986**, *19*, 2501.
(48) Goodby, J. W.; Dummur, D. A.; Collings, P. J. *Liq. Cryst.* **1995**, *19*, 703.
(49) de Gennes, P.-G. *Scaling Concepts in Polymer Physics*; Cornell University Press: Ithaca, New York, 1979.
(50) Nojima, S.; Roe, R.-J. *Macromolecules* **1987**, *20*, 1866.
(51) Nojima, S.; Kato, K.; Yamamoto, S.; Ashida, T. *Macromolecules* **1992**, *25*, 2237.
(52) For example, Goodby, J. W. In *Handbook of Liquid Crystals*; Demus, D., Goodby, J., Gray, G. W., Spiess, H.-W., Vill, V., Eds; Wiley-VCH: Weinheim, 1998; Vol. 1, pp 115−132.
(53) Schoen, A. H. *NASA Tech. Note* **1970**, No. D-5541.
(54) Andersson, S.; Hyde, S. T.; Larsson, K.; Lidin, S. *Chem. Rev.* **1988**, *88*, 221.
(55) Hyde, S. T.; Andersson, S.; Ericsson, B.; Larsson, K. *Z. Kristallogr.* **1984**, *168*, 213.
(56) Clerc, M.; Dubois-Violette, E. *J. Phys. II France* **1994**, *4*, 275.
(57) Fogden, A.; Lidin, S. *J. Chem. Soc., Faraday Trans.* **1994**, *90*, 3423.
(58) Charvolin, J. *Mol. Cryst. Liq. Cryst.* **1991**, *198*, 145.
(59) Chung, H.; Caffrey, M. *Biophys. J.* **1994**, *66*, 377.
(60) Nishino, Y.; Yano, S.; Tansho, M.; Yamaguchi, T. *Chem. Phys. Lett.* **1998**, *296*, 408.
(61) Göring, P.; Diele, S.; Fisher, S.; Wiegeleben, A.; Pelzl, G.; Stegemeyer, H.; Thyen, W. *Liq. Cryst.* **1988**, *25*, 467.